Development of a Multineedle Electroresistivity Probe for Measuring Bubble Characteristics in Molten Metal Baths

MANABU IGUCHI, TADATOSHI NAKATANI, and HIROTOSHI KAWABATA

Precise information on the behavior of rising bubbles in molten metals is of essential importance for the enhancement of current metal-refining processes as well as the development of new refining processes agitated by gas injection. In particular, the total interfacial area between bubbles and molten metal is a key parameter, but it cannot be evaluated unless the shape of bubbles is given. Getting information on the shape of rising bubbles has been very difficult for nontransparent liquids. In this study, we developed a multineedle electroresistivity probe to detect the shape of bubbles rising in molten metal baths. The accuracy of the presently developed probe was examined for water-air and Wood's metal-He systems using a conventional two-needle electroresistivity probe and a high-speed video camera.

I. INTRODUCTION

IT is widely recognized that the behavior of bubbles rising in the reactors of material-refining processes agitated by gas injection plays an essential role for the efficiency of the processes.[1–5] Theoretical and experimental investigations on the bubble behavior, therefore, have been carried out by many researchers on the basis of various kinds of cold and hot models. The bubble characteristics specified by gas holdup α, bubble frequency f_B, mean bubble rising velocity $\overline{u}_B$, and mean bubble chord length $\overline{L}_B$ can be measured with a two-needle electroresistivity probe which has been used extensively in this research field.[6–13] It should be noted that the first two values can be measured with a one-needle electroresistivity probe as well.

Although metallurgical reactions between molten metal and bubbles in a bath are significantly influenced by the total gas-liquid interfacial area, the conventional two-needle electroresistivity probe cannot give us any information on the bubble shape, which is closely associated with the total interfacial area. Even an X-ray fluoroscope cannot give us detailed information on the shape of bubbles. It can detect only the contour of a bubble. Considering these circumstances, we decided to develop a multineedle electroresistivity probe capable of detecting the shape of bubbles in addition to the aforementioned gas holdup, bubble frequency, mean bubble rising velocity, and mean bubble chord length. It is said that a prototype of this kind of multineedle probe has been developed by Davenport *et al.*[14] to detect a single cap-shape bubble rising in mercury.

The accuracy of a newly developed multineedle electroresistivity probe was first examined using an aqueous system. Experimental results of the gas holdup, bubble frequency, mean bubble rising velocity, and mean bubble chord length were compared satisfactorily with their respective values obtained using a two-needle electroresistivity probe. The shape of each bubble detected with the multineedle electroresistivity probe was very similar to that observed with a high-speed video camera. The multineedle electroresistivity probe was subsequently applied to a Wood's metal-He system to clarify the shape of inert gas bubbles in molten metal baths.

MANABU IGUCHI, formerly Associate Professor, Faculty of Engineering, Osaka University, is Professor, Division of Materials Science and Engineering, Graduate School of Engineering, Hokkaido University, Hokkaido, 060 Japan. TADATOSHI NAKATANI, Graduate Student, and HIROTOSHI KAWABATA, Technician, Faculty of Engineering, are with Osaka University, Osaka, 565 Japan.

Manuscript submitted March 12, 1996.

II. EXPERIMENTAL APPARATUS AND MEASUREMENT METHOD

A. *Water-Air System*

Figure 1 shows a schematic diagram of the experimental apparatus for an aqueous system. The cylindrical vessel made of transparent acrylic resin had an inner diameter D of 200 mm and a height H of 390 mm. Water was filled at a depth H_L of 250 mm. In many cases, air was injected through a centered single-hole bottom nozzle with an inner diameter d_n of 0.5 mm. Some additional measurements were carried out for d_n = 2 mm. The temperature of the air was controlled to become the same as that of the water in the bath, *i.e.*, 25 °C. Accordingly, it was not necessary to take bubble expansion due to temperature difference into consideration. The air flow rate Q_g was adjusted with a mass flow controller.

1. *Two-needle electroresistivity probe*

The bubble characteristics specified by gas holdup α, bubble frequency f_B, mean bubble rising velocity $\overline{u}_B$, and mean bubble chord length $\overline{L}_B$ were measured with a two-needle electroresistivity probe for more than 2 minutes. A stainless steel wire with a diameter of 0.5 mm and acrylic resin were used as the electrode needle and insulator, respectively. As shown in Figure 2 (*a*), each electrode needle was covered with acrylic resin except at its tip. Counter electrodes were immersed along the sidewall in order not to disturb the flow field in the bath. The vertical distance L_p between the tips of the two electrode needles was 2 mm. The output signals of the two-needle electroresistivity probe were A/D converted at a sampling frequency of 5 kHz and subsequently processed on a personal computer.

The mean bubble rising velocity $\overline{u}_B$ and mean bubble chord length $\overline{L}_B$ were calculated from the following equa-

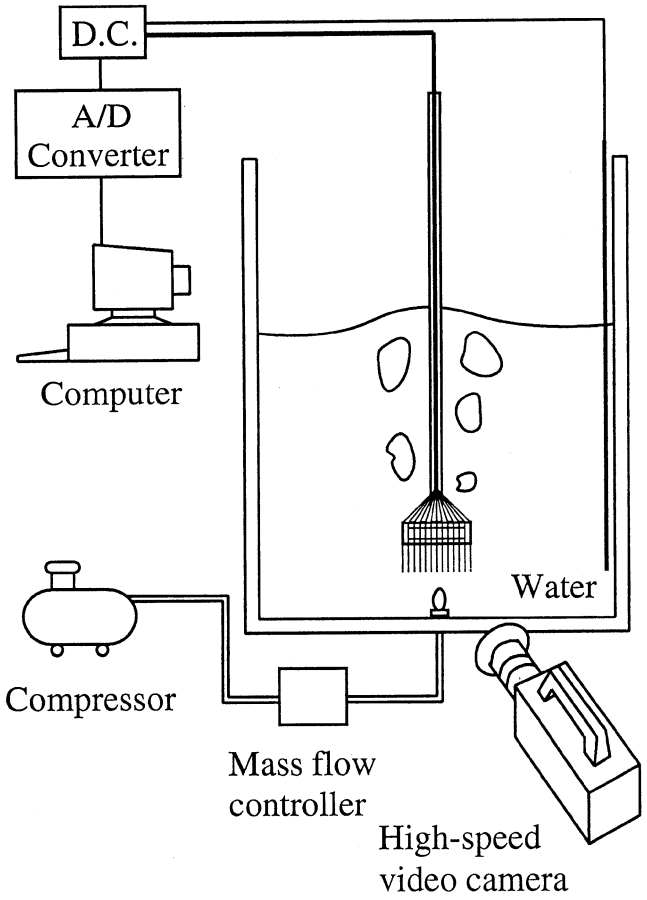

Fig. 1—Experimental apparatus for water-air system.

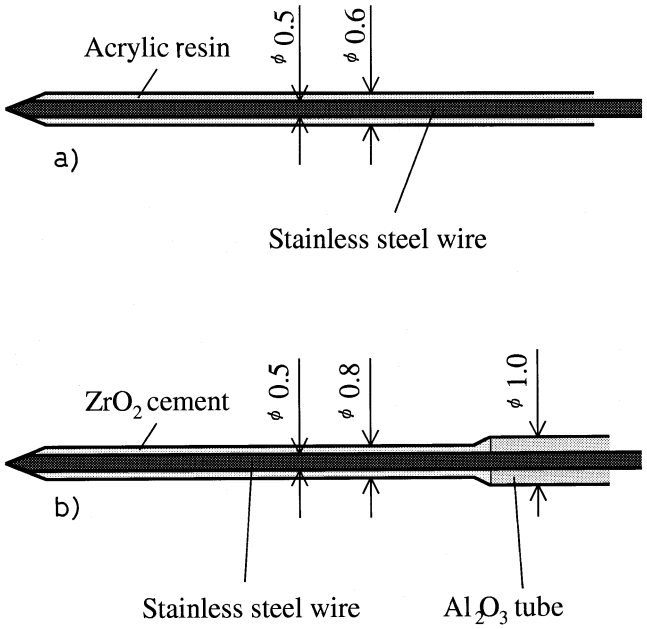

Fig. 2—Schematic of electrode needle: (*a*) water-air system and (*b*) Wood's metal-He system.

tions:

$$\overline{u}_B = \Sigma u_{Bi}/N \quad [1]$$

$$\overline{L}_B = \Sigma L_{Bi}/N \quad [2]$$

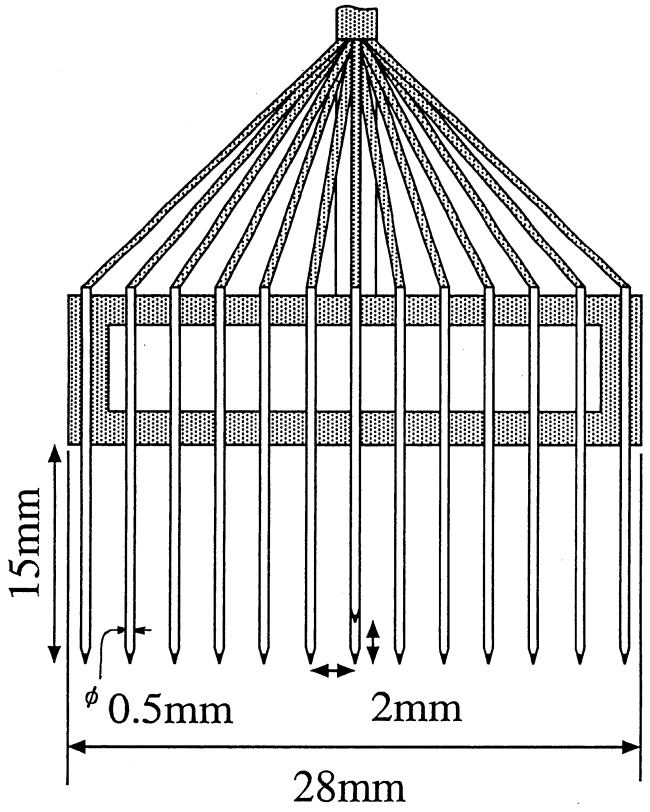

Fig. 3—Schematic of multineedle electroresistivity probe.

where the subscript i denotes the ith bubble signal and N denotes the total number of bubble signals. In this analysis, only bubble signals satisfying the following condition were discriminated and stored on a personal computer to calculate the mean values of $\overline{u}_B$ and $\overline{L}_B$:

$$0.7 < t_{Bu}/t_{BL} < 1.3 \quad [3]$$

where t_{Bu} and t_{BL} are bubble passing times at the upper and lower electrode needles, respectively. More than 1000 bubble signals ($N > 1000$) were stored. The determination of the limit values of 0.7 and 1.3 in Eq. [3] and other details of the two-needle electroresistivity probe and the data processing method are referred to in the previous article.[13]

2. *High-speed video camera*

The vertical shape of bubbles was recorded with a high-speed video camera at 250 frames per second.

3. *Multineedle electroresistivity probe*

Figure 3 shows a schematic of the presently developed multineedle electroresistivity probe. Thirteen needles made of stainless steel wire with a diameter of 0.5 mm were placed with equal intervals of 2 mm. One more needle was placed along the central needle so that the vertical distance between the tips of the two needles was 2 mm. These two central needles were used to determine the bubble rising velocity u_B, where the subscript i was deleted for the sake of simplicity. The total number of electrode needles, therefore, was 14. This is because 14 channels are available for the A/D converter used here.

The surface of each needle was covered with acrylic resin except at its tip, in the same manner as for the two-needle electroresistivity probe. The output signal of each

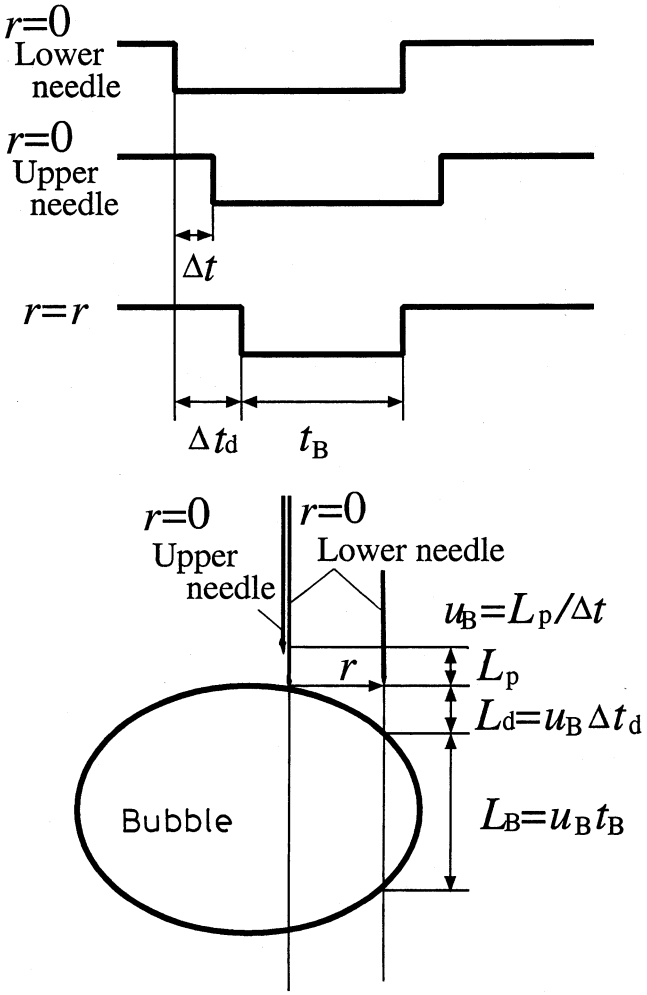

Fig. 4—Measurement method of bubble shape.

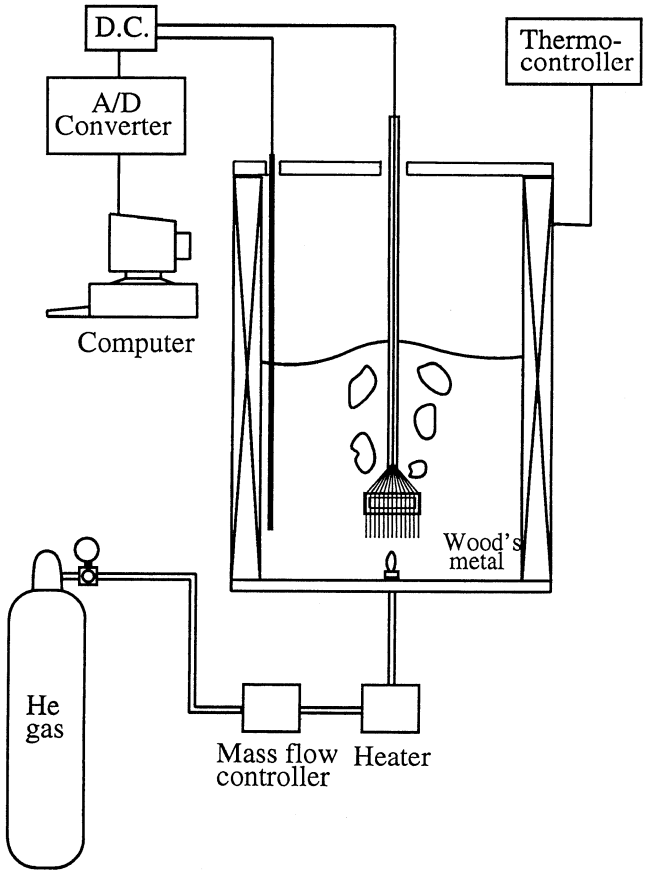

Fig. 5—Experimental apparatus for Wood's metal-He system.

needle was processed at a sampling frequency of 1 kHz. The time delay for data acquisition between the first electrode needle (left end in Figure 3) and the fourteenth (right end) was 0.4 ms. The mean bubble rising velocity was approximately 60 cm/s under the present experimental conditions. Each bubble rose approximately 0.24 mm during 0.4 ms. This vertical distance was less than 3 pct of the mean bubble chord length and hence, the time delay of 0.4 ms was acceptable for detecting the shape of bubbles satisfactorily. More than 1000 bubble signals were stored to determine $\overline{u}_B$.

In this study, the rising velocity of every part of a bubble was assumed to be uniform. That is, the bubble rising velocity u_B was represented by a value determined with the lower and upper central needles placed on the centerline of the bath. The bubble chord length L_B at each radial measurement position ($r = r$) can be calculated from

$$L_B = u_B t_B \quad [4]$$

where t_B is the passing time of the bubble, as shown in Figure 4.

In addition, the relative axial distance L_d between the forward bubble-liquid interface detected by the lower central needle located at $r = 0$ and that detected by the needle located at $r = r$ can be determined from

$$L_d = u_B \Delta t_d \quad [5]$$

where Δt_d is the time delay between the bubble signals obtained at $r = 0$ and $r = r$. We can readily determine the vertical shape of the bubble using the data on L_B and L_d.

B. *Wood's Metal-He System*

A schematic of the experimental apparatus for the Wood's metal-He system is shown in Figure 5. The cylindrical test vessel made of stainless steel had an inner diameter D of 200 mm and a height H of 300 mm. Wood's metal with a melting temperature of 70 °C (343 K) was heated to 105 °C (378 K) in the bath. The bath depth H_L was kept at 150 mm. The density, kinematic viscosity, and surface tension of the Wood's metal are $\rho_L = 9.56$ g/cm^3, $\nu_L = 0.341$ mm^2/s, and $\sigma = 460$ mN/m, respectively. Helium gas was preheated with a heater placed upstream of a single-hole bottom nozzle with an inner diameter d_n of 0.5 mm and, subsequently, injected into the Wood's metal bath through the nozzle at the same temperature as the bath. Such a small nozzle diameter was chosen to prevent the weeping of molten Wood's metal in the nozzle. The He gas flow rate was adjusted by the mass flow controller used for the aqueous system.

As mentioned previously, the air flow rate was 66 N cm^3/s (at STP), while the He flow rate was 60 N cm^3/s, where STP represents the standard temperature and pressure. These normal gas flow rates were chosen to yield almost the same volumetric gas flow rate at the nozzle exit in the two systems.

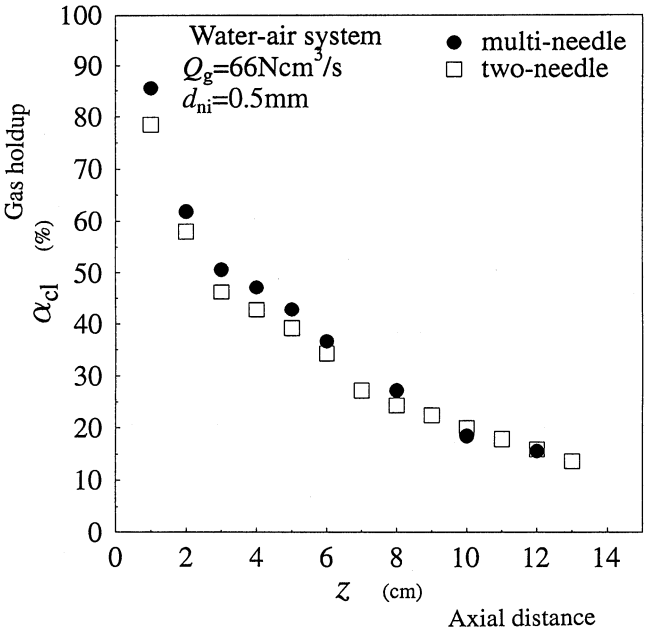

Fig. 6—Centerline values of gas holdup for water-air system.

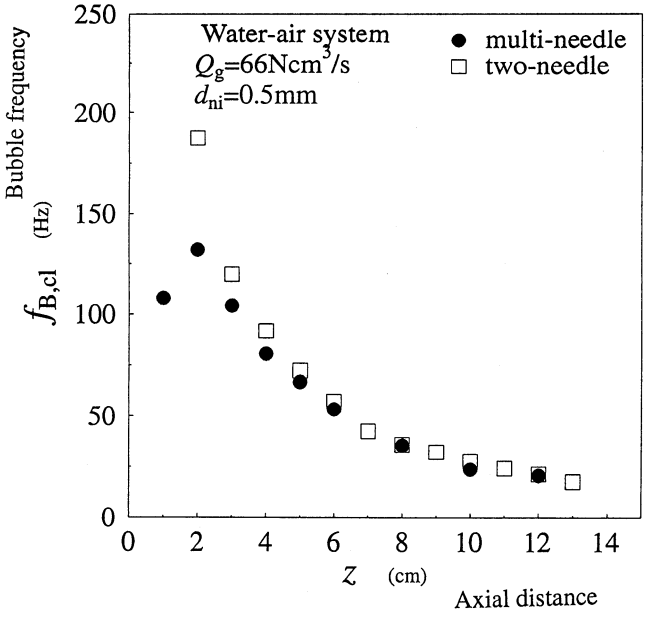

Fig. 7—Centerline values of bubble frequency for water-air system.

A stainless steel wire was also used as the electrode needle for the Wood's metal-He system, while ZrO_2 cement was used as the insulator, as shown in Figure 2(b). The shape and size of the multineedle electroresistivity probe are the same as those shown in Figure 3. The same materials were used for the two-needle electroresistivity probe. According to previous investigations,[15,16,17] this multineedle electroresistivity probe would be applicable to molten iron and molten copper of temperatures lower than approximately 1300 °C. For these molten metals of temperatures higher than 1300 °C, we should choose more adequate materials for the electrode needles and insulator.[11,15–17]

The output signals of the two-needle and multineedle electroresistivity probes were processed in the same manner as for the water-air system. Time of more than 2 minutes was necessary to get sufficient data for statistical treatment.

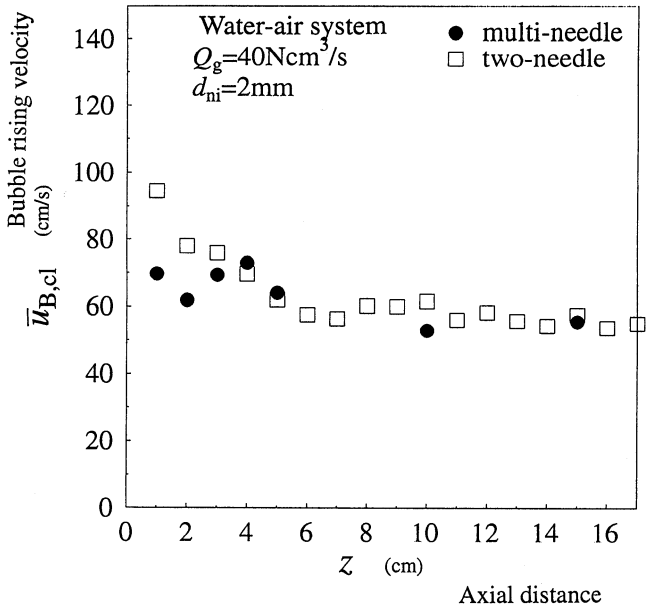

Fig. 8—Centerline values of mean bubble rising velocity for water-air system.

III. EXPERIMENTAL RESULTS AND DISCUSSION

A. *Water-Air System*

Measured values of gas holdup and bubble frequency on the centerline of the bath, α_{cl} and $f_{B,cl}$, are shown in Figures 6 and 7, respectively. The measured values of α_{cl} for the two kinds of electroresistivity probes agreed with each other within a scatter of ± 10 pct everywhere in the bath. Meanwhile, the multineedle electroresistivity probe brings about less accurate results of bubble frequency in the vicinity of the nozzle exit ($z \lesssim 2$ cm). This seems attributable partly to a relatively low sampling frequency, *i.e.*, relatively low temporal resolution for the multineedle electroresistivity probe. Since the capacity of the A/D converter used in this study is limited, the sampling frequency for each needle is 1 kHz, which is considerably lower than the 5 kHz for the two-needle electroresistivity probe. Another reason for the difference is that the multineedle probe confines and distorts the flow when placed close to the nozzle.

Data on the mean bubble rising velocity on the centerline, $\overline{u}_{B,cl}$, and mean bubble chord length on the centerline, $\overline{L}_{B,cl}$, obtained for a different air flow rate of 40 N cm^3/s and a nozzle inner diameter of 2 mm are shown in Figures 8 and 9, respectively. In each figure, agreement between measured values obtained with the two kinds of electroresistivity probes is good except near the nozzle exit.

The radial distributions of gas holdup α and bubble frequency f_B measured at $z = 5$ cm under the same blowing condition for the results in Figures 6 and 7 are given in Figures 10 and 11, respectively. The multineedle electroresistivity probe was fixed so that its lower central needle overlapped the centerline of the bath, as shown in Figure 1. Accordingly, all data were obtained with different elec-

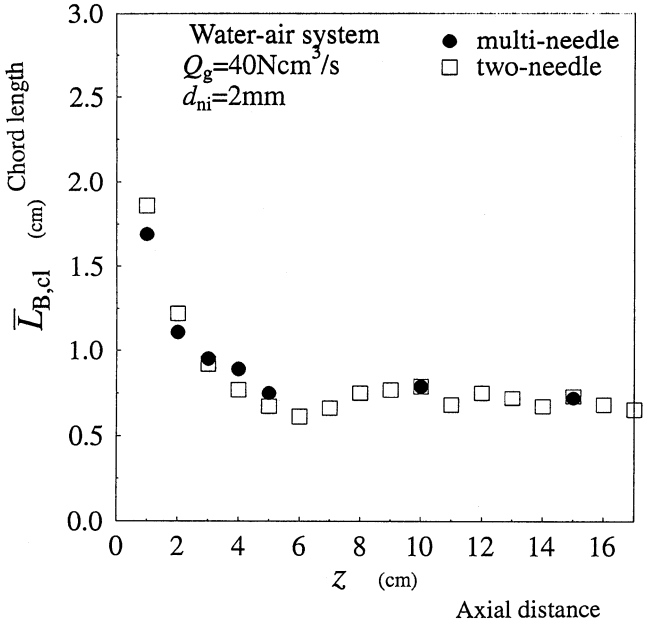

Fig. 9—Centerline values of mean bubble chord length for water-air system.

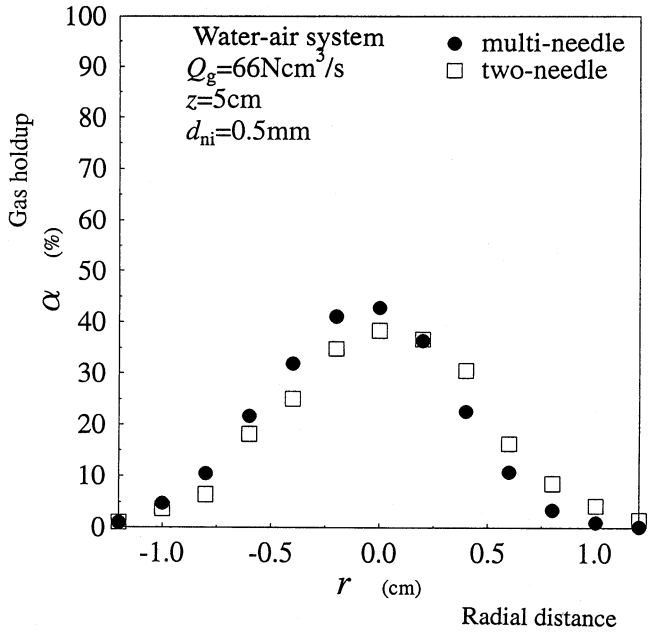

Fig. 10—Radial distributions of gas holdup measured at z = 5 cm for water-air system.

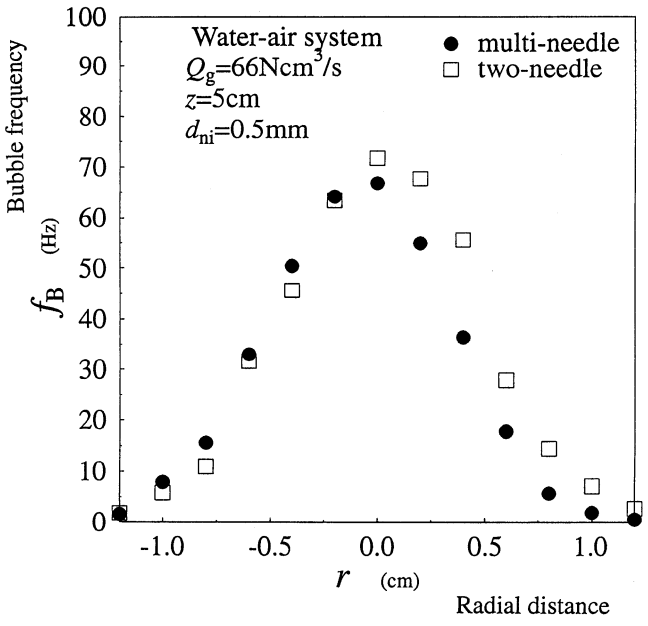

Fig. 11—Radial distributions of bubble frequency measured at z = 5 cm for water-air system.

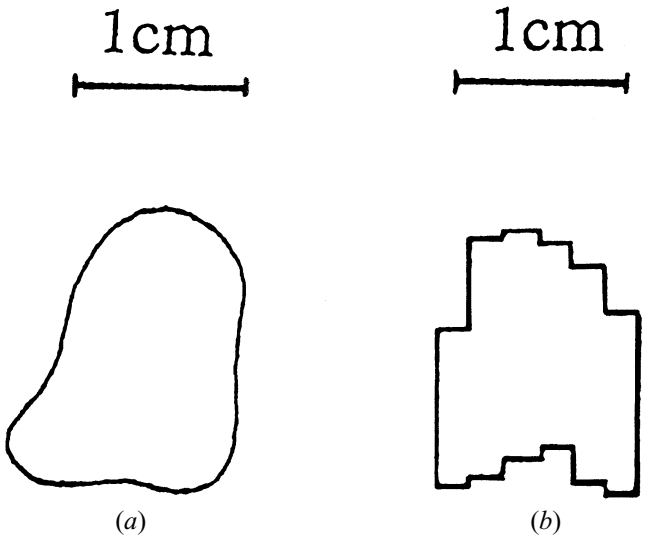

Fig. 12—Measured bubble shape for water-air system: (*a*) high-speed video camera and (*b*) multineedle electroresistivity probe.

trode needles, while the two-needle electroresistivity probe was traversed in the radial direction with equal intervals of 2 mm. At every radial measurement position, the measured values for the two kinds of electroresistivity probes almost agreed with each other. Accordingly, the behavior of rising bubbles was not influenced by the number of electrode needles. Both the radial distributions of α and f_B almost followed Gaussian distributions as widely accepted for bubbling jets under the present experimental conditions.[12,13]

The present multineedle electroresistivity probe was found to be useful in the whole bath except near the nozzle exit. Provided that the sampling frequency for each needle of the multineedle electroresistivity probe is raised and the size of each needle is minimized, this probe would yield more accurate results even near the nozzle exit.

Figure 12 compares the vertical shape of a bubble observed for d_n = 0.5 mm, Q_g = 66 N cm^3/s, and z = 3 cm using a high-speed video camera with that detected using the presently developed multineedle electroresistivity probe. The bubble shapes shown in Figures 12(a) and (b) are close to each other. It should, however, be stressed that the high-speed video camera gives us the vertical contour line of the bubble, whereas the multineedle electroresistivity probe gives not the vertical contour line but the vertical cross section of the bubble. This result also supports the adequacy of the present multineedle electroresistivity probe. Although the evidence is not given here, the mean bubble rising velocity $\overline{u}_B$ was almost uniform for $r < 1$ cm.

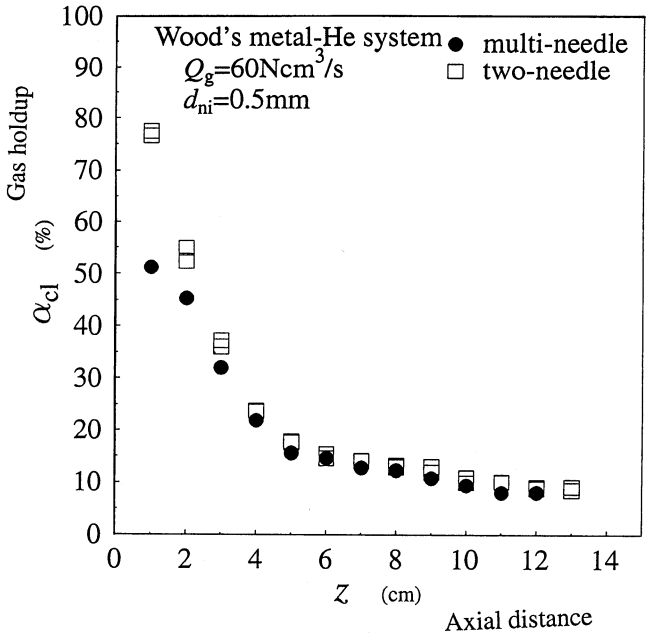

Fig. 13—Centerline values of gas holdup for Wood's metal-He system.

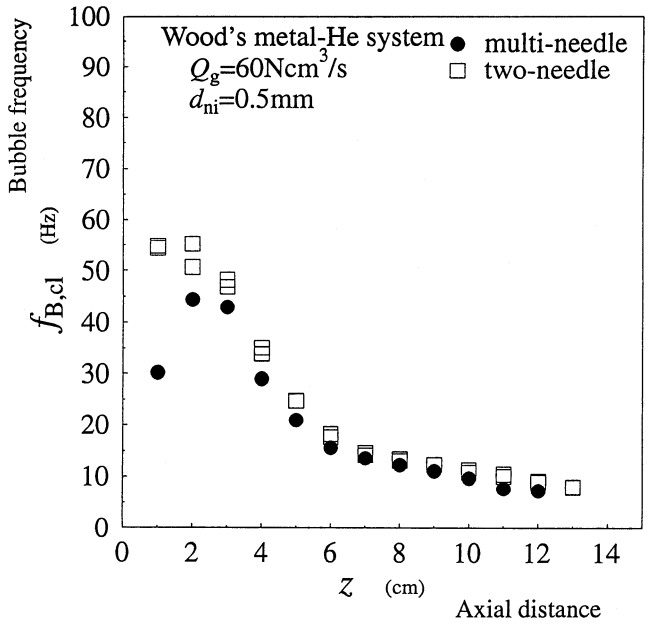

Fig. 14—Centerline values of bubble frequency for Wood's metal-He system.

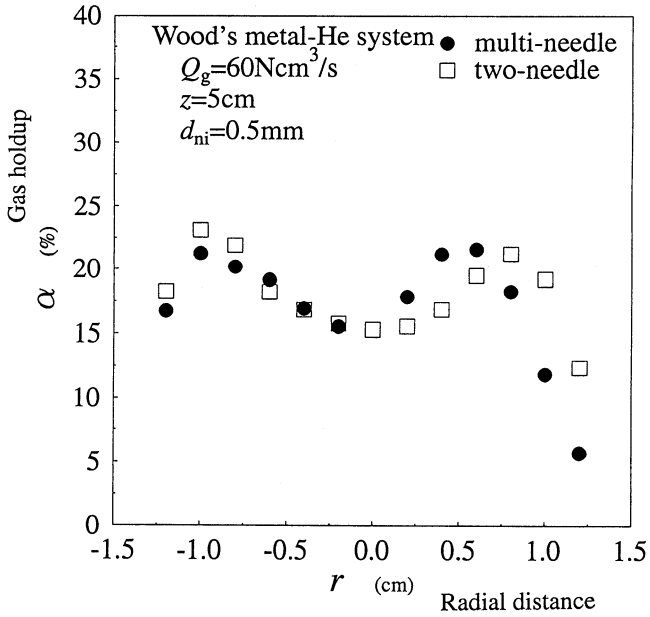

Fig. 15—Radial distributions of gas holdup measured at z = 5 cm for Wood's metal-He system.

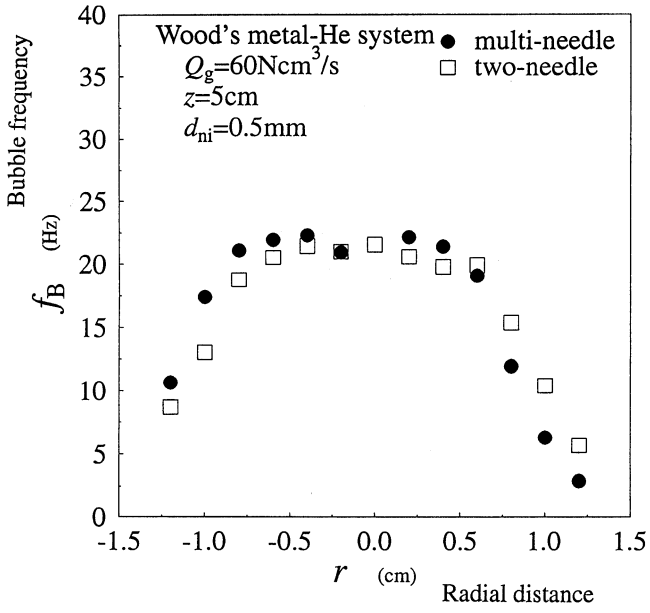

Fig. 16—Radial distributions of bubble frequency measured at z = 5 cm for Wood's metal-He system.

The validity of the aforementioned assumption for $\overline{u}_B$, therefore, was confirmed.

B. *Wood's Metal-He System*

Figures 13 and 14 show the centerline values of the gas holdup α and bubble frequency f_B, respectively. In each figure, agreement between the results for the two kinds of probes are reasonably good except near the nozzle exit. Just like the water-air system, the present multineedle electroresistivity probe is applicable to the Wood's metal-He system except near the nozzle exit ($z \lesssim 2$ cm).

The radial distribution of gas holdup at z = 5 cm is illustrated in Figure 15. Unlike the radial distribution of gas holdup for the water-air system at the same volumetric gas flow rate, the radial distribution of α has two peaks. A similar radial distribution can be observed when a swirl motion of a bubbling jet occurs in a relatively shallow bath of $0.3 \lesssim H_L/D \lesssim 1$,[18] where H_L is the bath depth and D is the bath diameter. This kind of swirl motion resembles the rotary sloshing appearing in a cylindrical vessel, which is subject to horizontal or vertical external forced oscillation. In the presence of the swirl motion, the radial distribution of bubble frequency f_B also is known to have two peaks.[19] The radial distribution of f_B, however, is almost uniform near the centerline, as shown in Figure 16. In addition, the swirl motion was not observed by eye inspection under this experimental condition. The radial distributions

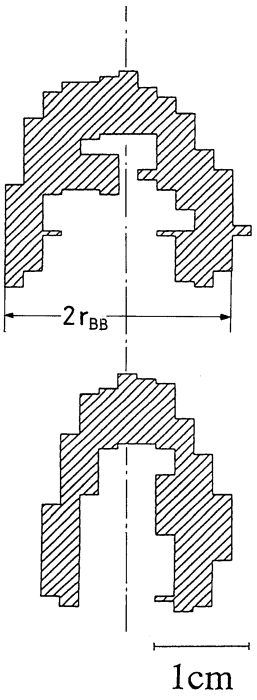

Fig. 17—Bubble shape of two successively rising bubbles detected at z = 5 cm with multineedle electroresistivity probe for Wood's metal-He system.

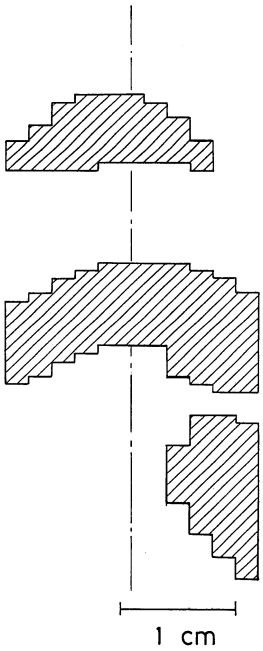

Fig. 18—Bubble shape of three successively rising bubbles detected at z = 8 cm with multineedle electroresistivity probe for Wood's metal-He system.

of α and f_B shown in Figures 15 and 16, therefore, are not associated with the swirl motion of a bubbling jet.

According to Figures 15 and 16, most bubbles exist for $\gamma \lesssim 1.3$ cm.

The cross sections of two successively rising bubbles are illustrated in Figure 17. The mean bubble rising velocity $\overline{u}_B$ was assumed to be uniform in the radial direction in determining the shape of bubbles, but actual $\overline{u}_B$ values obtained by the two-needle electroresistivity probe changed slightly (<10 pct) in that direction. A more precise cross section of each bubble can be obtained by modifying the cross section shown in Figure 17 using the local $\overline{u}_B$ value. The modified cross sections, however, are not shown here because there is little difference between the original and modified cross sections.

The bubbles shown in Figure 17 are reasonably regarded as being axisymmetrical with respect to their vertical axis, and bubble shape is skirted. A vertical bubble cross section similar to those shown in Figure 17 can be seen when a relatively large isolated bubble rises in a transparent high kinematic viscosity and low surface tension liquid at rest.[20] In the present case, however, the kinematic viscosity is low and the surface tension is high, and bubbles are generated almost periodically. Each bubble is affected in the course of rising by turbulent molten metal flow induced by preceding bubbles. This is the main reason for the difference between bubble shapes in still aqueous systems and the present system.

It is worth noting again that even an X-ray fluoroscope cannot detect precisely the vertical cross section of a bubble.[21,22]

The bottom radius r_{BB} of each bubble shown in Figure 17 is approximately 1 cm, which is almost identical to the outer edge of the bubble dispersion region ($\lesssim$ 1.3 cm) estimated from the radial distributions of α and f_B shown in Figures 15 and 16. These facts imply that each bubble rises around z = 5 cm, hardly fluctuating in the radial direction. Measured gas holdup values, therefore, would be approximately proportional to the bubble chord length L_B. According to Figure 17, the chord length of each bubble has a maximum near the outer edge. This might be the reason for two peaks appearing on the radial distribution of α. On the other hand, since the bubble frequency f_B is not dependent on the chord length, f_B is expected to be almost uniform near the centerline of the bath. This is true, as can be seen in Figure 16.

According to water model experiments, bubbles rising in an axial region far from the nozzle exit are disturbed by highly turbulent motion of liquid caused by the wake of preceding bubbles, and hence, disintegration of the bubbles takes place. In Figure 18, three successively rising bubbles observed at z = 8 cm are illustrated. The skirted bubble shape is not observed anymore, probably due to the disintegration of bubbles.

IV. CONCLUSIONS

1. A multineedle electroresistivity probe was developed to measure the bubble characteristics specified by gas holdup α, bubble frequency f_B, mean bubble rising velocity $\overline{u}_B$, and mean bubble chord length $\overline{L}_B$ and to detect the vertical shape of bubbles rising in transparent as well as nontransparent liquids. The accuracy of this probe was confirmed by comparing experimental results for the bubble characteristics in a water-air system and in a Wood's metal-He system with those measured with a conventional two-needle electroresistivity probe. In addition, the vertical shape of bubbles detected by the multineedle electroresistivity probe for the water-air system

was favorably compared with that observed with a high-speed video camera. The presently developed multineedle electroresistivity probe was found to be useful in the whole bath except near the nozzle exit for the water-air and Wood's metal-He systems.

2. Helium bubbles successively generated in the Wood's metal bath were skirted above the nozzle exit ($z = 5$ cm) under the present blowing conditions. Disintegration of the bubbles took place far from the nozzle exit ($z = 8$ cm). The radial distributions of gas holdup α were found to be closely associated with the shape of bubbles.

Judging from the previous experimental evidence, the multineedle electroresistivity probe developed in this study for the Wood's metal-He system would be applicable to molten iron and molten copper of temperatures less than approximately 1300 °C. If a platinum electrode needle covered with ZrO_2 cement is used as the electrode and alumina (Al_2O_3) as the insulator, this multineedle electroresistivity probe is considered to be useful even for a molten iron bath at a temperature of 1600 °C.

REFERENCES

1. K. Mori and M. Sano: *Tetsu-to-Hagané*, 1981, vol. 67, pp. 672-95.
2. J. Szekely, G. Carlson, and L. Helle: *Ladle Metallurgy*, Springer, Secaucus, NY, 1989.
3. Y. Sahai and G.R. St. Pierre: *Advances in Transport Processes in Metallurgical Systems*, Elsevier, New York, NY, 1992.
4. M. Iguchi, F. Yamamoto, T. Uemura, and Z. Morita: *Jpn. J. Multiphase Flow*, 1992, vol. 6, pp. 54-64.
5. D. Mazumder and R.I.L. Guthrie: *Iron Steel Inst. Jpn. Int.*, 1995, vol. 35, pp. 1-20.
6. M. Kawakami, N. Tomimoto, and K. Itoh: *Tetsu-to-Hagané*, 1982, vol. 68, pp. 774-83.
7. T.H. Tacke, H.G. Schubert, D.J. Weber, and K. Schwerdtfeger: *Metall. Trans. B.*, 1985, vol. 16B, pp. 263-75.
8. S. Taniguchi, A. Kikuchi, H. Matsuzaki, and N. Bessho: *Trans. Iron Steel Inst. Jpn.*, 1988, vol. 28, pp. 262-70.
9. A.H. Castillejos and J.K. Brimacombe: *Metall. Trans. B*, 1989, vol. 20B, pp. 595-601.
10. Y.K. Xie, S. Orsten, and F. Oeters: *Proc. IISC*, 1990, vol. 1, pp. 421-28.
11. M. Kawakami, S. Hosono, K. Takahashi, and K. Itoh: *Tetsu-to-Hagané*, 1992, vol. 78, pp. 267-74.
12. M. Iguchi, K. Nozawa, and Z. Morita: *Iron Steel Inst. Jpn. Int.*, 1991, vol. 31, pp. 952-59.
13. M. Iguchi, K. Nozawa, H. Tomida, and Z. Morita: *Iron Steel Inst. Jpn. Int.*, 1992, vol. 32, pp. 747-53.
14. W.G. Davenport, F.D. Richardson, and A.V.B. Bradshaw: *Chem. Eng. Sci.*, 1967, vol. 22, pp. 1221-35.
15. M. Iguchi, H. Kawabata, Z. Morita, K. Nakajima, and Y. Itoh: *Iron Steel Inst. Jpn. Int.*, 1994, vol. 34, pp. 980-85.
16. M. Iguchi, H. Kawabata, K. Nakajima, and Z. Morita: *Metall. Mater. Trans. B*, 1995, vol. 26B, pp. 67-74.
17. M. Iguchi, H. Kawabata, K. Nakajima, and Z. Morita: *Trans. Jpn. Soc. Mech. Eng.*, 1996, vol. 62 (593), pp. 79-84.
18. M. Iguchi, S. Hosohara, K. Koga, R. Yamaguchi, and Z. Morita: *Iron Steel Inst. Jpn. Int.*, 1993, vol. 33, pp. 1037-44.
19. M. Iguchi, S. Hosohara, T. Kondoh, Y. Itoh, and Z. Morita: *Iron Steel Inst. Jpn. Int.*, 1994, vol. 34, pp. 330-37.
20. R. Clift, J.R. Grace, and M.E. Weber: *Bubbles, Drops, and Particles*, Academic Press, New York, NY, 1978.
21. K.G. Davis, G.A. Irons, and R.I.L. Guthrie: *Metall. Trans. B*, 1978, vol. 9B, pp. 721-22.
22. M. Iguchi, T. Chihara, N. Takanashi, Y. Ogawa, N. Tokumitsu, and Z. Morita: *Iron Steel Inst. Jpn. Int.*, 1995, vol. 35, pp. 1354-61.